J Biomol NMR (2015) 63:237–244
DOI 10.1007/s10858-015-9985-9

COMMUNICATION

Speeding-up exchange-mediated saturation transfer experiments by Fourier transform

Marta G. Carneiro[1] · Jithender G. Reddy[1] · Christian Griesinger[1] · Donghan Lee[1,2]

Received: 24 June 2015 / Accepted: 2 September 2015 / Published online: 9 September 2015

Abstract Protein motions over various time scales are crucial for protein function. NMR relaxation dispersion experiments play a key role in explaining these motions. However, the study of slow conformational changes with lowly populated states remained elusive. The recently developed exchange-mediated saturation transfer experiments allow the detection and characterization of such motions, but require extensive measurement time. Here we show that, by making use of Fourier transform, the total acquisition time required to measure an exchange-mediated saturation transfer profile can be reduced by twofold in case that one applies linear prediction. In addition, we demonstrate that the analytical solution for $R_1\rho$ experiments can be used for fitting the exchange-mediated saturation transfer profile. Furthermore, we show that simultaneous analysis of exchange-mediated saturation transfer profiles with two different radio-frequency field strengths is required for accurate and precise characterization of the exchange process and the exchanging states.

Keywords CEST · Chemical exchange · DEST · Fourier transform · NMR · Protein dynamics

Electronic supplementary material The online version of this article (doi:10.1007/s10858-015-9985-9) contains supplementary material, which is available to authorized users.

✉ Donghan Lee
dole@nmr.mpibpc.mpg.de

[1] Department of NMR-based Structural Biology, Max-Planck Institute for Biophysical chemistry, Am Fassberg 11, 37077 Goettingen, Germany

[2] Department of Medicine, James Graham Brown Cancer Center, University of Louisville, 529 South Jackson Street, Louisville, KY 40202, USA

Conformational fluctuations play a key role in functions of biomolecules and hence numerous spectroscopic methods are used for their study. Among them, nuclear magnetic resonance spectroscopy (NMR) provides dynamic information with atomic resolution (Ban et al. 2013b; Mittermaier and Kay 2009; Palmer III 2004, 2014). Several NMR studies have linked sparsely populated states to functionality over different time scales—from nanosecond to milliseconds (Ban et al. 2011; Bhabha et al. 2011; Henzler-Wildman et al. 2007; Lange et al. 2008; Smith et al. 2015; Tzeng and Kalodimos 2012). Furthermore, a long-standing question on how the different time scale motions are hierarchically interconnected has been recently addressed via a population shuffling mechanism (Smith et al. 2015). These new findings are possible mainly due to developments in NMR relaxation dispersion experiments, which allow the characterization of conformational exchange in proteins, providing kinetic, thermodynamic, and structural information on lowly populated states in the microsecond–millisecond time scale (Ban et al. 2012, 2013a, b; Palmer III 2014; Smith et al. 2015; Vallurupalli et al. 2008). Specifically, recent developments have pushed the limits of such relaxation dispersion experiments towards motions as fast as 4 μs (Ban et al. 2012; Smith et al. 2015). On the other hand, slower motions with a very low populated conformation, such as monomer-fibril exchange, can be studied by methods based on exchange-mediated saturation transfer, namely chemical exchange saturation transfer (CEST) (Vallurupalli et al. 2012) and dark state exchange saturation transfer (DEST) (Fawzi et al. 2011). Both methods rely on the observation that for a system undergoing chemical exchange, perturbation of one of the states by radio-frequency irradiation will be transferred to the interconverting state (Mayer and Meyer 1999; Ward et al. 2000). Thus, when the irradiation is applied to the on-

resonance position of the lowly populated (minor) state peak, the intensity of the highly populated (major) state peak will be decreased. Intensity changes in the major state peak are monitored as a function of frequency offset to yield the exchange-mediated saturation transfer (CEST or DEST) profile. These experiments provide a wealth of information about the exchanging system: not only the exchange parameters (population of the minor species and exchange rate), but also the chemical shift of the minor species and residue-specific longitudinal and transverse relaxation rates can be extracted by fitting to the appropriate models. Here we describe a strategy to achieve reliable transverse relaxation rate constants, an aspect particularly crucial when studying equilibrium between rapidly and slowly tumbling species in solution—typically a monomeric protein and a very large assembly, such as an amyloid fibril. In addition, we present a new method based on Fourier transform (FT), which allows for a significant reduction in measurement time. To exemplify both methods, we have used the agglutinin of *Oscillatoria agardhii* (OAA), which binds to high-mannose glycans such as those found in the HIV's gp120 envelope protein. Previously measured CPMG relaxation dispersion at 277 K revealed that several residues undergo conformational exchange in the time scale targeted by CEST experiments (Carneiro et al. 2015).

Although CEST and DEST profiles are commonly analyzed using the numerical solution of the Bloch–McConnell equation (Fawzi et al. 2011; Vallurupalli et al. 2012; Zhao et al. 2014), these experiments can be treated as off-resonance $R_{1\rho}$ experiments (Palmer III 2014; Zaiss and Bachert 2013; Zhao et al. 2014) since the analytical solution for $R_{1\rho}$ relaxation rates is based on the largest eigenvalue of the Bloch–McConnell equation (Baldwin and Kay 2013; Trott and Palmer III 2002). Thus, both transverse and longitudinal magnetizations can be described with this eigenvalue. The use of this analytical approach provides some advantages over using the Bloch–McConnell equation (McConnell 1958) in terms of computational speed and insight into the relationship between different experimental and fitting parameters.

Table 1 and Fig. 1 summarize the fitting of CEST profiles of four representative residues of OAA (Val 38, Asn 75, Trp 77, and Asn 104) to either the $R_{1\rho}$ analytical solution or to the Bloch–McConnell equation. Both the fitting parameters and the quality of the fit obtained using the analytical solution are comparable to the ones obtained using the Bloch–McConnell equation, demonstrating the applicability of both models. In addition, the exchange parameters [exchange rate (k_{ex}), population of the minor state (p_b), and chemical shift difference between the major and the minor states ($\Delta\delta$)] are in agreement with the ones previously obtained by ^{15}N CPMG relaxation dispersion for Asn 75 and Trp 77 (Carneiro et al. 2015). Of note, the CEST profiles of Val 38 and Asn 104, which display flat CPMG relaxation dispersion curves (data not shown), reveal the presence of chemical exchange. The fitted values of k_{ex} and p_b (Table 1) indicate that these residues undergo

Table 1 Fitting parameters obtained from CEST experiments measured for four residues of OAA with two radio-frequency field strengths (15 and 75 Hz) to either the analytical solution derived for $R_{1\rho}$ relaxation or to the Bloch–McConnell equation

	Analytical	Bloch–McConnell
Val 38		
k_{ex} (s^{-1})	100 ± 28	94 ± 25
p_b (%)*	0.6 ± 0.2	0.6 ± 0.2
$\Delta\delta$ (ppm)	−2.43 ± 0.06	−2.44 ± 0.05
R_2^a (s^{-1})	25.6 ± 0.2	25.7 ± 0.2
R_2^b (s^{-1})	134 ± 29	109 ± 31
R_1 (s^{-1})**	0.391 ± 0.002	0.390 ± 0.002
Reduced χ^2	1.14	1.13
Asn 75		
k_{ex} (s^{-1})	342 ± 40	326 ± 39
p_b (%)*	2.6 ± 0.4	2.8 ± 0.4
$\Delta\delta$ (ppm)	2.28 ± 0.07	2.28 ± 0.07
R_2^a (s^{-1})	20.7 ± 0.7	20.8 ± 0.7
R_2^b (s^{-1})	26 ± 17	24 ± 14
R_1 (s^{-1})**	0.556 ± 0.009	0.556 ± 0.009
Reduced χ^2	0.38	0.38
Trp 77		
k_{ex} (s^{-1})	279 ± 33	258 ± 30
p_b (%)*	2.9 ± 0.4	3.2 ± 0.5
$\Delta\delta$ (ppm)	6.48 ± 0.06	6.48 ± 0.07
R_2^a (s^{-1})	26.5 ± 0.9	26.7 ± 0.8
R_2^b (s^{-1})	79 ± 27	70 ± 29
R_1 (s^{-1})**	0.63 ± 0.01	0.63 ± 0.01
Reduced χ^2	0.69	0.68
Asn 104		
k_{ex} (s^{-1})	112 ± 21	106 ± 21
p_b (%)*	0.5 ± 0.1	0.6 ± 0.1
$\Delta\delta$ (ppm)	2.40 ± 0.07	2.41 ± 0.07
R_2^a (s^{-1})	23.9 ± 0.2	24.0 ± 0.2
R_2^b (s^{-1})	102 ± 19	84 ± 19
R_1 (s^{-1})**	0.403 ± 0.003	0.403 ± 0.002
Reduced χ^2	0.98	0.98

* CEST profiles were fitted assuming a two-state model, such that $p_a + p_b = 1$

** The longitudinal relaxation rate (R_1) is assumed to be the same for both states

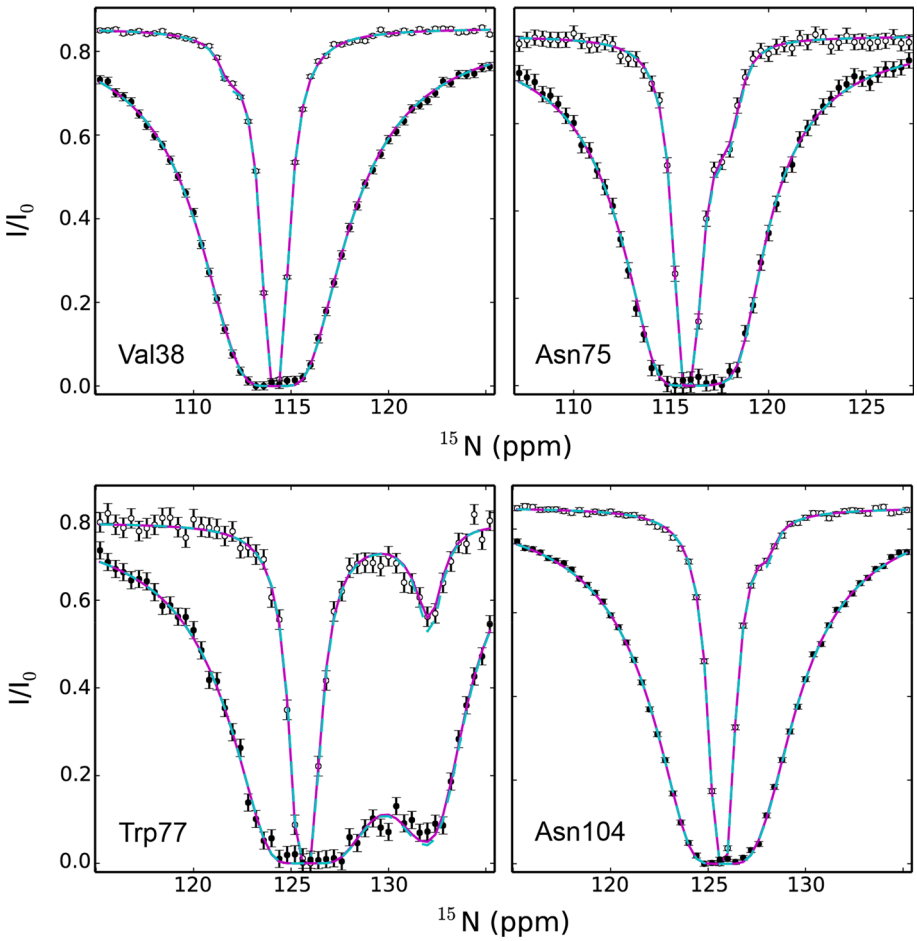

Fig. 1 Comparison between fitting results using the analytical solution and the Bloch–McConnell equation. CEST profiles are shown for residues Val 38, Asn 75, Trp 77, and Asn 104 of the anti-HIV lectin OAA, which display slow motions at 277 K. For each residue, the data collected with the two radio-frequency field strengths (15 and 75 Hz, *open* and *filled circles*, respectively) was simultaneously fitted to either the analytical solution derived for $R_{1\rho}$ relaxation or to the Bloch–McConnell equation. The best fits to the analytical solution are shown in *magenta*, *solid lines* and the best fits to the numerical solution are shown in *cyan*, *dashed lines*

chemical exchange with a very lowly populated conformation ($p_b \approx 0.5$ %) and in the slow time scale window ($k_{ex} \approx 100\ s^{-1}$) which is challenging for relaxation dispersion experiments (Vallurupalli et al. 2012).

While the chemical shift difference can be readily inferred from visual inspection of the CEST profile and the longitudinal relaxation rate (R_1) is easily estimated from the I/I_0 ratio (see Methods), the exchange parameters rely on model fitting to the experimental data. A comparison of the fitting results of CEST profiles with a single or two different radio-frequency strengths (Fig. 2; Table 2) indicates that a single radio-frequency field strength is not enough to estimate properly all parameters, with k_{ex} and the transverse relaxation rate of the minor state (R_2^b) being the most affected. Even though the quality of the individual fits is very similar to the simultaneous fit of two radio-frequency field strengths (Fig. 2), k_{ex} and R_2^b assume very different values (Table 2), indicating that these parameters are interdependent. In order to identify the experimental parameters that can be manipulated to obtain reliable k_{ex} and R_2^b values we examined the $R_{1\rho}$ analytical solution derived by Baldwin and Kay (Eq. 1) (Baldwin and Kay 2013):

$$R_{1\rho} = C_{R1}R_1\cos^2\theta + \left(C_{R2}R_2^a + R_{ex}\right)\sin^2\theta \qquad (1)$$

where $\cos^2\theta = ((\delta_a - \delta_{RF}) + p_b\Delta\delta)^2/(\nu_1^2 + ((\delta_a - \delta_{RF}) + p_b\Delta\delta)^2)$ and $\sin^2\theta = \nu_1^2/(\nu_1^2 + ((\delta_a - \delta_{RF}) + p_b\Delta\delta)^2)$; $\Delta\delta = \delta_b - \delta_a$; ν_1 is the applied radio-frequency field strength, p_b is the population of the minor state, $\delta_{a/b}$ is the resonance frequency of the major (a) or minor (b) state and δ_{RF} is the resonance frequency at which the radio-frequency field ν_1 is applied.

The magnitude of the *sin* term is proportional to ν_1 and, in the limit of very weak field strengths, the *sin* term is negligible and only the *cos* term contributes significantly to $R_{1\rho}$. The coefficient C_{R1} (Eq. 2) has explicit contributions from the intrinsic transverse relaxation rate of the major (R_2^a) and the minor (R_2^b) states and from the exchange rate (k_{ex}):

$$C_{R1} = \frac{k_{ex}^2 + v_1^2 + (\delta_a - \delta_{RF})^2(\delta_b - \delta_{RF})^2/((\delta_a - \delta_{RF}) + p_b\Delta\delta)^2 + \left(c_1 + (c_2 - c_3)\left(R_2^b - R_2^a\right)\right)\tan^2\theta}{k_{ex}^2 + \left(v_1^2 + (\delta_a - \delta_{RF})^2\right)\left(v_1^2 + (\delta_b - \delta_{RF})^2\right)/\left(v_1^2 + ((\delta_a - \delta_{RF}) + p_b\Delta\delta)^2\right) + c_2\left(R_2^b - R_2^a\right)\sin^2\theta} \quad (2)$$

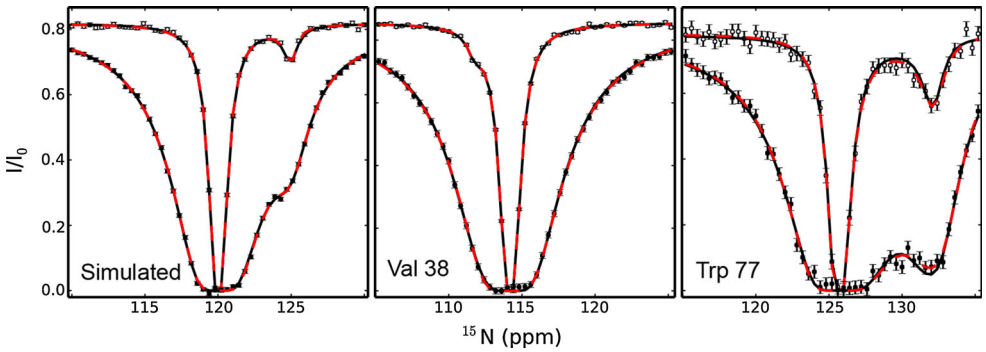

Fig. 2 Simultaneous fit of CEST profiles using two different radio-frequency field strengths is necessary for precise and accurate determination of the fitting parameters. CEST profiles using two different radio-frequency field strengths (15 Hz, *open circles*; 75 Hz, *filled circles*) were simulated using k_{ex}, p_b, δ_a, δ_b, R_1, R_2^a, and R_2^b of 150 s^{-1}, 1 %, 120 ppm, 125 ppm, 0.5, 20.0, and 100.0 s^{-1}, respectively. Experimental CEST profiles using the same radio-frequency field strengths are also shown for Val 38 and Trp 77 of OAA. The best fit of the CEST profiles on a per residue and per field strength basis to the analytical solution is shown in *red dashed line*. The best fit of the CEST profiles on a per residue basis (i.e., simultaneous fit of both radio-frequency field strengths) is shown in *black solid line*

Again, the *sin* and *tan* terms in Eq. (2) are proportional to ν_1 and, in the limit, are negligible (for simplicity the coefficients associated with these terms are denoted as c_1, c_2, and c_3. A full description of these terms can be found in the Supporting Information). Thus, with weak radio-frequency field strengths, the measured effect is nearly independent of R_2.

A larger contribution from R_2 can be found in the coefficients of the *sin* term in Eq. (1) (C_{R2} and R_{ex}; Eqs. (3) and (4), respectively):

$$C_{R2} = \frac{c_4 + c_3\left(R_2^b - R_2^a\right)}{c_5 + c_3\left(R_2^b - R_2^a\right)\sin^2\theta} \quad (3)$$

$$R_{ex} = \frac{c_1 k_{ex} + c_6\left(R_2^b - R_2^a\right)}{c_5 + c_3\left(R_2^b - R_2^a\right)\sin^2\theta} \quad (4)$$

where c_4, c_5, and c_6 denote terms dependent on the exchange parameters, whose full description is provided in the Supporting Information. The contribution of the *sin* term in Eq. (1) is therefore beneficial to define R_2^b, and can be augmented by using stronger radio-frequency field strengths. This requirement is elucidated using simulated CEST data (Table 2; Fig. 2), for which all parameters are known a priori. Using data with a single radio-frequency field (either 15 or 75 Hz) significantly impairs the estimation of k_{ex} and R_2^b, despite the overall good quality of the fit (reduced χ^2 of 0.8 and 1.0 for 15 and 75 Hz, respectively). Conversely, the simultaneous fit of data with both radio-frequency field strengths leads to accurate and precise estimation of all parameters (Table 2). The same conclusion could also be drawn with the experimentally measured CEST profiles (Table 2; Fig. 2). The combination of a weak radio-frequency field (15 Hz or less) with a stronger radio-frequency field (75 Hz or more) enables the accurate determination k_{ex} and R_2^b over the range of exchange parameters usually targeted by CEST experiments (Figure S1).

In addition to the requirement of more than one radio-frequency field strengths, the numerous frequency offsets measured for exchange-mediated saturation transfer profiles result in extensive measurement time, which can hinder the study of various important metastable systems. In an attempt to reduce the total acquisition time necessary for exchange-mediated saturation transfer experiments, we compare the results obtained using CEST profiles for which a sparse number of frequency offsets are sampled (hereafter termed reduced CEST profiles) to the ones obtained using conventional CEST profiles, for which twice the number of frequency offsets are sampled. The reduced and conventional CEST profiles for four different residues of OAA are shown in Fig. 3 and the extracted fitting parameters are summarized in Table 3. While $\Delta\delta$, p_b, R_2^a, R_1, are

Table 2 Simultaneous fit of CEST profiles with two different radio-frequency field strengths is necessary for precise and accurate determination of the fitting parameters

	ν_1 = 15 Hz	ν_1 = 75 Hz	ν_1 = 15 and 75 Hz
Simulated*			
k_{ex} (150 s^{-1})	174 ± 43	72 ± 83	143 ± 7
p_b (1 %)**	0.9 ± 0.3	2 ± 2	1.02 ± 0.06
Δδ (5 ppm)	5.0 ± 0.4	4.95 ± 0.09	4.99 ± 0.02
R_2^a (20 s^{-1})	19.8 ± 0.4	20.9 ± 0.9	20.2 ± 0.2
R_2^b (100 s^{-1})	32 ± 39	65 ± 29	103 ± 8
R_1 (0.5 s^{-1})***	0.505 ± 0.004	0.50 ± 0.01	0.500 ± 0.003
Reduced χ^2	0.81	1.01	0.93
Val 38			
k_{ex} (s^{-1})	209 ± 65	903 ± 3535	101 ± 28
p_b (%)**	0.5 ± 0.2	2 ± 378	0.6 ± 0.2
Δδ (ppm)	−2.52 ± 0.07	−1 ± 1	−2.43 ± 0.06
R_2^a (s^{-1})	24.9 ± 0.5	28 ± 37	25.6 ± 0.2
R_2^b (s^{-1})	35 ± 62	0 ± 19	134 ± 29
R_1 (s^{-1})***	0.392 ± 0.002	0.39 ± 0.02	0.391 ± 0.002
Reduced χ^2	1.94	0.43	1.14
Trp 77			
k_{ex} (s^{-1})	340 ± 99	531 ± 116	279 ± 33
p_b (%)**	3 ± 1	2.1 ± 0.6	2.9 ± 0.4
Δδ (ppm)	6.5 ± 0.1	6.7 ± 0.2	6.48 ± 0.06
R_2^a (s^{-1})	24 ± 4	24 ± 4	26.5 ± 0.9
R_2^b (s^{-1})	77 ± 129	0 ± 40	79 ± 27
R_1 (s^{-1})***	0.62 ± 0.02	0.64 ± 0.05	0.63 ± 0.01
Reduced χ^2	0.48	0.78	0.69

Fitting parameters extracted from individual fit of CEST profiles with two different radio-frequency field strengths (15 or 75 Hz) and from simultaneous fit with the two radio-frequency field strengths (15 and 75 Hz), using the analytical solution

* Parameters used to simulate the CEST profiles are shown in parenthesis

** CEST profiles were fitted assuming a two-state model, such that $p_a + p_b = 1$

*** The longitudinal relaxation rate (R_1) is assumed to be the same for both states

comparable for both data sets, k_{ex} and R_2^b can differ significantly between the two data sets. Residues undergoing conformational exchange with very slow exchange rates, small chemical shift differences and highly skewed populations (such as Val 38 and Asn 75) are particularly affected. The reduced CEST profiles of these residues Fig. 3; Val 38 and Asn 104 show a minute, hardly recognizable, "dip" at the resonance offset corresponding to the minor state chemical shift, and the fitted k_{ex} and R_2^b deviate from the ones obtained for the conventional data sets. In addition, the parameters derived from the reduced data sets are less precise (higher fractional error) than the ones obtained from the conventional data set (Table S1), though the fitting accuracy (in terms of reduced χ^2) is comparable in most cases (Table 3). In order to retain the advantages of reduced measurement time without impairing the estimation of the parameters extracted from exchange-mediated saturation transfer profiles, we developed a strategy to extend a reduced profile using Fourier transform (FT).

Analogous to continuous wave (CW) NMR spectroscopy, the acquisition of a CEST profile requires the entire scanning of large spectral windows, with a series of 2D ^{1}H, ^{15}N spectra being recorded as a weak radio frequency field (ν_1) is applied at varying ^{15}N offsets. As mentioned before, the intensity of a peak of interest is monitored as a function of the frequency offset at which the weak ν_1 field was applied, to yield the CEST profile (Vallurupalli et al. 2012). Thus, CEST profiles are in essence frequency domain spectra and can be converted into a time-domain signal using inverse FT (Hoch and Stern 1996). The time domain signal is now amenable to standard linear prediction (LP) algorithms commonly used to process NMR data (Hoch and Stern 1996). The extrapolated time domain signal is then reconverted into a frequency domain spectrum by FT. In order to determine whether this type of processing can overcome the limitations noted above for the reduced CEST profiles, we have applied it to the reduced data sets and compared the results to the ones obtained using conventional data sets. The reduced CEST profiles were converted into a time domain signal using inverse FT, and subsequently extended to twice the number of frequency offsets (that is, the FT processed profiles have the same number of frequency offsets as the conventional profiles) using a standard LP algorithm (see Supporting Information). Given the small number of input data points, the LP extrapolation is limited to a factor of two (Hoch and Stern 1996). Following the LP processing step the time domain signal was converted back into a frequency domain spectrum using FT. The resulting FT and LP processed profiles (hereafter termed FT-CEST profile) are shown in Fig. 3. For all four residues, the FT-CEST profiles are comparable to the conventional ones, for which all data points were experimentally acquired. More importantly, the fitting parameters obtained from the FT-CEST profiles are similar to the ones obtained from the conventional method (Table 3). In particular, k_{ex} and R_2^b, which were compromised when reduced profiles were used, are in good agreement with the values obtained from the conventional data sets. It should be noted that, as LP improves only the resolution of typical NMR spectra, the use of LP in the exchange-mediated saturation transfer profile improves only the definition of the minor "dip".

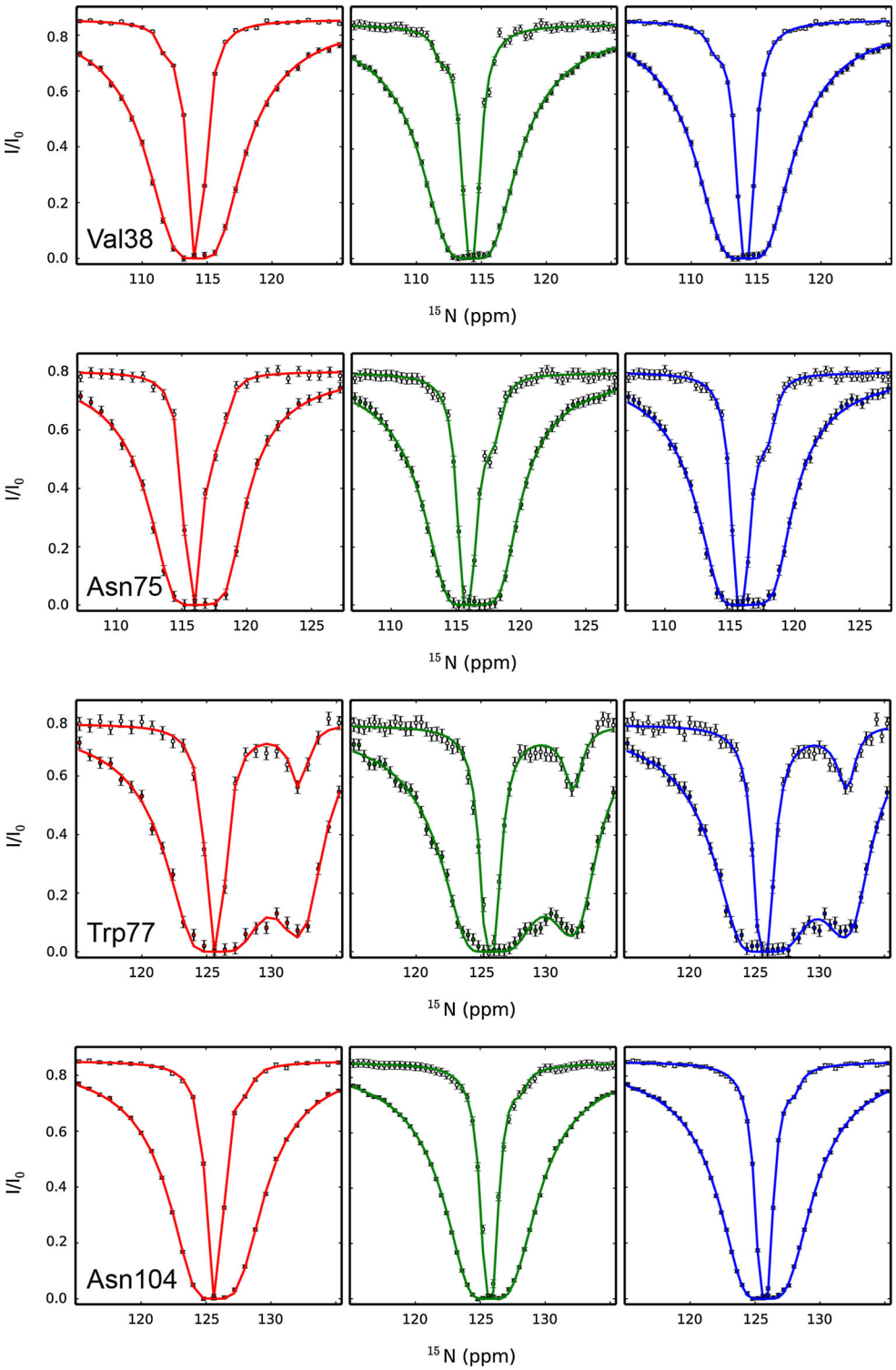

Fig. 3 Conventional CEST profiles can be reproduced by Fourier transform and linear prediction extrapolation of reduced datasets. Reduced CEST profile (56 Hz per frequency offset increment; *red*), FT-CEST profile obtained by FT and subsequent LP processing of the reduced dataset (*green*) and conventional CEST profile (28 Hz per frequency offset increment; *blue*) for Val 38, Asn 75, Trp 77, and Asn 104 of OAA. The data was acquired using two ν_1 field strengths (15 Hz, *open circles* and 75 Hz, *filled circles*). *Solid lines* correspond to the best simultaneous fit of the profiles for $\nu_1 = 15$ and 75 Hz

The improvements in the estimation of the exchange parameters (in particular k_{ex} and R_2^b) result from the better definition of the minor dip (Figure S2).

In summary, we show that simultaneous analysis of CEST profiles with two different radio-frequency field strengths is necessary for accurately estimating all fitting parameters, especially the exchange rate and the transverse relaxation rate of the minor state. In addition, we present a new method, based on Fourier transform and linear prediction, which reduces the measurement time required for exchange-mediated saturation transfer experiments by a factor of two. The method is exemplified using CEST

Table 3 FT-CEST fitting results are comparable to conventional CEST

	Reduced	FT	Conventional
Val 38			
k_{ex} (s^{-1})	55 ± 43	93 ± 46	100 ± 28
p_b (%)*	0.8 ± 0.8	0.6 ± 0.4	0.6 ± 0.2
Δδ (ppm)	−2.32 ± 0.07	−2.4 ± 0.1	−2.43 ± 0.06
R_2^a (s^{-1})	25.5 ± 0.6	25.6 ± 0.5	25.6 ± 0.2
R_2^b (s^{-1})	97 ± 47	106 ± 40	134 ± 29
R_1 (s^{-1})**	0.392 ± 0.003	0.394 ± 0.006	0.391 ± 0.002
Reduced χ^2	1.32	0.72	1.14
Asn 75			
k_{ex} (s^{-1})	360 ± 57	347 ± 41	342 ± 40
p_b (%)*	2.6 ± 0.6	2.6 ± 0.5	2.6 ± 0.4
Δδ (ppm)	2.28 ± 0.09	2.29 ± 0.07	2.28 ± 0.07
R_2^a (s^{-1})	20 ± 1	20.5 ± 0.7	20.7 ± 0.7
R_2^b (s^{-1})	29 ± 26	29 ± 18	26 ± 17
R_1 (s^{-1})**	0.55 ± 0.01	0.55 ± 0.01	0.556 ± 0.009
Reduced χ^2	0.33	0.44	0.38
Trp 77			
k_{ex} (s^{-1})	286 ± 43	262 ± 28	279 ± 33
p_b (%)*	2.8 ± 0.5	2.9 ± 0.4	2.9 ± 0.4
Δδ (ppm)	6.57 ± 0.09	6.50 ± 0.07	6.48 ± 0.06
R_2^a (s^{-1})	26 ± 1	26.5 ± 0.9	26.5 ± 0.9
R_2^b (s^{-1})	56 ± 39	83 ± 28	79 ± 27
R_1 (s^{-1})**	0.63 ± 0.02	0.63 ± 0.01	0.63 ± 0.01
Reduced χ^2	0.82	0.93	0.69
Asn 104			
k_{ex} (s^{-1})	81 ± 38	91 ± 35	112 ± 21
p_b (%)*	0.5 ± 0.3	0.5 ± 0.2	0.5 ± 0.1
Δδ (ppm)	2.6 ± 0.1	2.5 ± 0.4	2.40 ± 0.07
R_2^a (s^{-1})	24.2 ± 0.2	24.0 ± 0.3	23.9 ± 0.2
R_2^b (s^{-1})	59 ± 25	112 ± 44	102 ± 19
R_1 (s^{-1})**	0.402 ± 0.004	0.397 ± 0.006	0.403 ± 0.003
Reduced χ^2	0.95	1.11	0.98

Fitting parameters obtained from the analysis of CEST experiments for Val 38, Asn 75, Trp 77, and Asn 104 of OAA, using a reduced dataset, an FT-extended dataset and a conventional dataset

* CEST profiles were fitted assuming a two-state model, such that $p_a + p_b = 1$

** The longitudinal relaxation rate (R_1) is assumed to be the same for both states

profiles, but the same principles apply for DEST experiments. Our strategy enables improved characterization of the minor state and shorter acquisition times. These advantages over the conventional method are particularly important for the study of metastable systems, such as amyloid proteins.

Acknowledgments The authors thank L. M. I. Koharudin and A. M. Gronenborn for kindly providing ^{15}N-labeled OAA sample. We also thank G. Bouvignies and L. E. Kay for providing a software to validate our in-house software for fitting CEST profiles. This work was supported by the James Graham Brown Foundation, the Max Planck Society and the EU (ERC Grant Agreement Number 233227 to CG).

References

Baldwin A, Kay L (2013) An R1ρ expression for a spin in chemical exchange between two sites with unequal transverse relaxation rates. J Biomol NMR 55:211–218

Ban D et al (2011) Kinetics of conformational sampling in ubiquitin. Angw Chem Int Ed Engl 50:11437–11440

Ban D, Gossert AD, Giller K, Becker S, Griesinger C, Lee D (2012) Exceeding the limit of dynamics studies on biomolecules using high spin-lock field strengths with a cryogenically cooled probehead. J Magn Reson 221:1–4

Ban D et al (2013a) Enhanced accuracy of kinetic information from CT-CPMG experiments by transverse rotating-frame spectroscopy. J Biomol NMR 57:73–82

Ban D, Sabo T, Griesinger C, Lee D (2013b) Measuring dynamic and kinetic information in the previously inaccessible Supra-tc window of nanoseconds to microseconds by solution NMR spectroscopy. Molecules 18:11904–11937

Bhabha G et al (2011) A dynamic knockout reveals that conformational fluctuations influence the chemical step of enzyme catalysis. Science 332:234–238

Carneiro MG et al (2015) Sampling of glycan-bound conformers by the anti-HIV lectin *oscillatoria agardhii* agglutinin in the absence of sugar. Angw Chem, Int Ed Engl 54:6462–6465

Delaglio F, Grzesiek S, Vuister GW, Zhu G, Pfeifer J, Bax A (1995) NMRPipe: a multidimensional spectral processing system based on UNIX pipes. J Biomol NMR 6:277–293

Fawzi NL, Ying J, Ghirlando R, Torchia DA, Clore GM (2011) Atomic-resolution dynamics on the surface of amyloid-beta protofibrils probed by solution NMR. Nature 480:268–272

Helmus J, Jaroniec C (2013) Nmrglue: an open source Python package for the analysis of multidimensional NMR data. J Biomol NMR 55:355–367

Henzler-Wildman KA et al (2007) Intrinsic motions along an enzymatic reaction trajectory. Nature 450:838–844

Hoch JC, Stern AS (1996) NMR data processing. Wiley-Liss, New York

Keller RLJ (2004) The computer aided resonance assignment tutorial. CANTINA Verlag, Goldau

Koharudin LMI, Furrey W, Gronenborn AM (2011) Novel fold and carbohydrate specificity of the potent anti-HIV cyanobacterial lectin from *Oscillatoria agardhii*. J Biol Chem 286:1588–1597

Lange OF et al (2008) Recognition dynamics up to microseconds revealed from an RDC-derived ubiquitin ensemble in solution. Science 320:1471–1475

Mayer M, Meyer B (1999) Characterization of ligand binding by saturation transfer difference NMR spectroscopy. Angw Chem Int Ed Engl 38:1784–1788

McConnell HM (1958) Reaction rates by nuclear magnetic resonance. J Chem Phys 28:430–431

Mittermaier AK, Kay LE (2009) Observing biological dynamics at atomic resolution using NMR. Trends Biochem Sci 34:601–611

Palmer AG III (2004) NMR characterization of the dynamics of biomacromolecules. Chem Rev 104:3623–3640

Palmer AG III (2014) Chemical exchange in biomacromolecules: past, present, and future. J Magn Reson 241:3–17

Smith CA et al (2015) Population shuffling of protein conformations. Angw Chem Int Ed Engl 54:207–210

Trott O, Palmer AG III (2002) R1ρ relaxation outside of the fast-exchange limit. J Magn Reson 154:157–160

Tzeng S-R, Kalodimos CG (2012) Protein activity regulation by conformational entropy. Nature 488:236–240

Vallurupalli P, Hansen DF, Kay LE (2008) Structures of invisible, excited protein states by relaxation dispersion NMR spectroscopy. Proc Natl Acad Sci 105:11766–11771

Vallurupalli P, Bouvignies G, Kay LE (2012) Studying "Invisible" excited protein states in slow exchange with a major state conformation. J Am Chem Soc 134:8148–8161

Ward KM, Aletras AH, Balaban RS (2000) A new class of contrast agents for MRI based on proton chemical exchange dependent saturation transfer (CEST). J Magn Reson 143:79–87

Zaiss M, Bachert P (2013) Exchange-dependent relaxation in the rotating frame for slow and intermediate exchange—modeling off-resonant spin-lock and chemical exchange saturation transfer. NMR Biomed 26:507–518

Zhao B, Hansen AL, Zhang Q (2014) Characterizing slow chemical exchange in nucleic acids by carbon CEST and low spin-lock field R1ρ NMR spectroscopy. J Am Chem Soc 136:20–23